

# Structural and Dynamical Anomalies of a Gaussian Core Fluid: a Mode Coupling Theory Study

Lindsey Ann Shall and S. A. Egorov

*Department of Chemistry, University of Virginia,*

*Charlottesville, Virginia 22901, USA*

## Abstract

We present a theoretical study of transport properties of a liquid comprised of particles interacting via Gaussian Core pair potential. Shear viscosity and self-diffusion coefficient are computed on the basis of the mode-coupling theory, with required structural input obtained from integral equation theory. Both self-diffusion coefficient and viscosity display anomalous density dependence, with diffusivity increasing and viscosity decreasing with density within a particular density range along several isotherms below a certain temperature. Our theoretical results for both transport coefficients are in good agreement with the simulation data.

## I. INTRODUCTION

Liquids comprised of particles interacting via a Gaussian Core (GC) model pair potential have been receiving a lot of attention recently.[1–16] Strong theoretical interest in GC model stems from the fact that this bounded potential is useful for describing interactions between inherently penetrable entities, such as polymer coils.[13, 15] As such, both thermodynamic[3, 16] and dynamic[5–11] properties of GC fluids and binary mixtures have been extensively studied. It has been found that their transport coefficients exhibit anomalous behavior strongly reminiscent of waterlike model systems[17–26], with diffusivity increasing and viscosity decreasing with density over a certain range of thermodynamic conditions. Furthermore, a strong correlation between this behavior and structural anomalies quantified via excess entropy has been demonstrated.[9–11] Both structural and dynamical anomalous behavior has been rationalized in terms of bounded nature of GC potential which results in increasing amount of interparticle overlap with increasing density. In view of the above, it would be of interest to provide a firm theoretical link between structural and transport properties of GC fluid on the basis of microscopic statistical mechanical theory. Such a connection has been recently established for waterlike model systems[26] by combining integral equation theory of structure with mode-coupling theory (MCT) treatment of dynamics. The goal of the present work is to develop a similar treatment for the GC model. We show that integral equation theory/MCT combination is indeed capable of capturing anomalous behavior of transport coefficients of both neat GC fluids and binary mixtures observed in molecular dynamics (MD) simulations.[5–11] Our MCT-based microscopic analysis helps to shed further light on the origin and nature of transport anomalies. In particular, we are able to rationalize why viscosity anomaly persists over much more narrow range of densities and temperatures compared to the diffusion anomaly.

The remainder of the paper is organized as follows. In Section II we describe the microscopic model and review the MCT approach employed to calculate the transport coefficients. In Section III we compare theoretical results with the simulation data for the shear viscosity and the self-diffusion coefficient. In Section IV we conclude.

## II. MICROSCOPIC MODEL AND THEORY

We consider a system comprised of spherical particles interacting via isotropic GC pair potential  $\phi(r)$ :

$$\phi(r) = \epsilon \exp \left[ -(r/\sigma)^2 \right], \quad (1)$$

where the two parameters  $\epsilon$  and  $\sigma$  characterize the height and the width of the interaction profile, respectively. In the previous studies of the GC model, integral equation theory with the hypernetted chain (HNC) closure was shown to give reliable structural results for a wide range of densities studied.[3] Hence, we employ the HNC closure throughout this study to compute the radial distribution function  $g(r)$  for a liquid described by the GC pair potential. The validity of this approach will be further confirmed by comparing various structural quantities with the corresponding simulation data.

The main focus of the present work is the calculation of the transport properties of GC fluid and analysis of their anomalous behavior. We first describe our treatment of the self-diffusion coefficient. The latter is obtained from the total time integral of the time-dependent friction  $\zeta(t)$ : [27, 28]

$$D = \frac{k_B T}{m \zeta_0}, \quad (2)$$

with

$$\zeta_0 = \int_0^\infty dt \zeta(t). \quad (3)$$

The MCT result for the time-dependent friction reads:

$$\zeta(t) = \frac{k_B T \rho}{6\pi^2 m} \int_0^\infty dk k^4 c(k)^2 F(k, t) F_s(k, t) \quad (4)$$

where  $m$  is the mass of the fluid particle,  $T$  is the temperature,  $\rho$  is the number density, and  $c(k)$  is the fluid direct correlation function, which we obtain from the HNC closure. In the above,  $F(k, t)$  is the fluid dynamic structure factor, which we compute from the continued fraction representation of its Laplace transform truncated at the second order: [27, 29]

$$F(k, z) = \frac{S(k)}{z + \frac{\delta_1(k)}{z + \frac{\delta_2(k)}{z + \tau^{-1}(k)}}}, \quad (5)$$

where  $S(k)$  is the fluid static structure factor, and  $\delta_i(k)$  is the initial time value of the  $i^{\text{th}}$  order memory function (MF) of  $F(k, t)$ . For the parameter  $\tau^{-1}(k)$  we use the expression due

to Lovesey:[30]  $\tau^{-1}(k) = 2\sqrt{\delta_2(k)/\pi}$ . The quantities  $\delta_1(k)$  and  $\delta_2(k)$  can be easily calculated from the first three short-time expansion coefficients of  $F(k, t)$ ; the microscopic expressions for the latter are well-known and will not be reproduced here.[27, 29, 31] Finally,  $F_s(k, t)$  is the fluid self-dynamic structure factor, for which we have adopted a simple Gaussian model:[27, 28]

$$F_s(k, t) = \exp \left[ \frac{-k_B T k^2}{m \zeta_0} \left( t + \frac{1}{\zeta_0} e^{-t \zeta_0} - 1 \right) \right]. \quad (6)$$

Given that the self-dynamic structure factor is a function of  $\zeta_0$ , which, in turn, depends on  $F_s(k, t)$  via Eq. (4), Eqs. (4)-(6) need to be solved iteratively and self-consistently. One could use a more accurate model for  $F_s(k, t)$  in terms of the velocity time correlation function (TCF) of a tagged fluid particle,[32] but our numerical calculations have shown that this does not change the results for  $D$  in a noticeable way.

We note that the MCT result for the time-dependent friction given by Eq. (4) arises from coupling to collective density modes, and, as such, is only expected to be valid at intermediate to long times, i.e. it describes the slowly varying tail of  $\zeta(t)$ . At short times, one typically adopts an empirical approach by modeling the initial decay of the time-dependent friction via some rapidly decaying analytical function (e.g. a Gaussian), which is constructed in such a way as to preserve the exact short-time behavior of  $\zeta(t)$ . [27, 29] In particular, the exact result for the initial time value  $\zeta(0)$  reads:[27, 29]

$$\zeta(0) = \frac{4\pi\rho}{3m} \int_0^\infty dr r^2 g(r) \nabla^2 \phi(r). \quad (7)$$

At the same time, the zero-time value of the MCT expression for the time-dependent friction is given by:

$$\zeta(0)^{\text{MCT}} = \frac{k_B T \rho}{6\pi^2 m} \int_0^\infty dk k^4 c(k)^2 S(k) \quad (8)$$

By comparing the two expressions given by Eqs. (7) and (8) and by applying Parseval's theorem, one can see that the two results are equivalent under the random phase approximation (RPA),  $c(r) = -\phi(r)/k_B T$ . It has been shown in the previous studies of the GC liquid[13] that RPA is quite accurate in describing its structural properties. As such, MCT method provides essentially correct zero-time value of the time-dependent friction. Furthermore, numerical results presented in the next Section demonstrate that the MCT approach also describes the initial decay of  $\zeta(t)$  quite accurately. Hence, in the present work we do not decompose time-dependent friction into binary and collective terms, but rather employ

Eq. (4) at all times. As will be seen below, a similar situation occurs in the MCT treatment of the potential part of the shear stress autocorrelation function (SACF), which enters into the calculation of the shear viscosity.

The microscopic expression for the shear viscosity is given by the Green-Kubo formula in terms of the total time integral of the SACF (i.e. time-dependent shear viscosity  $\eta(t)$ ):[33]

$$\eta = \frac{1}{Vk_B T} \int_0^\infty dt \langle J_{xy}(t) J_{xy}(0) \rangle = \int_0^\infty dt \eta(t). \quad (9)$$

with the off-diagonal components of the stress tensor  $J_{xy}$  given by:

$$J_{xy} = \sum_{i=1}^N m v_i^x v_i^y - \sum_{i=1}^N \sum_{j>i}^N r_{ij}^x \frac{\partial \phi(r_{ij})}{\partial r_{ij}^y} = J_{xy}^k + J_{xy}^p \quad (10)$$

In the above,  $V$  is the total volume,  $N$  is the number of particles, lower indices  $i$  and  $j$  label the particles, while upper indices  $x$  and  $y$  denote the vector components of the particle velocities  $v_i$  and displacement vector  $r_{ij}$  connecting the particles  $i$  and  $j$ .

According to Eq. (10), the off-diagonal elements of the stress tensor are comprised of kinetic and potential terms,  $J_{xy}^k$  and  $J_{xy}^p$ , respectively. As a result, the SACF splits into three individual parts: potential-potential, kinetic-kinetic, and mixed kinetic-potential contributions:

$$\eta(t) = \eta_{pp}(t) + \eta_{kk}(t) + 2\eta_{kp}(t) = \frac{1}{Vk_B T} \left\{ \langle J_{xy}^p(t) J_{xy}^p(0) \rangle + \langle J_{xy}^k(t) J_{xy}^k(0) \rangle + 2 \langle J_{xy}^k(t) J_{xy}^p(0) \rangle \right\}, \quad (11)$$

with the shear viscosity coefficient given by the sum of the total time integrals of the three terms above:

$\eta = \eta_p + \eta_k + 2\eta_{kp}$ , where  $\eta_p = \int_0^\infty dt \eta_{pp}(t)$  etc. We now discuss the calculation of each of these terms in turn.

As in the case of the time-dependent friction, the MCT treatment of the potential term,  $\eta_{pp}(t)$ , involves coupling to collective density modes, and the corresponding result reads:[27, 29]

$$\eta_{pp}(t) = \frac{k_B T}{60\pi^2} \int_0^\infty dk k^4 \left[ \frac{S'(k)}{S(k)} \right]^2 \left\{ \left[ \frac{F(k, t)}{S(k)} \right]^2 \right\}, \quad (12)$$

where prime denotes differentiation with respect to the argument. In general, the above expression is used at intermediate and long times, while short-time behavior of  $\eta_{pp}(t)$  is modeled phenomenologically, based on its short-time expansion coefficients. The exact result

for the initial time value of  $\eta_{pp}(t)$  is given by:[27, 29]

$$\eta_{pp}(0) = \frac{2\pi}{15}\rho^2 \int_0^\infty dr g(r) \frac{d}{dr} \left[ r^4 \frac{d\phi(r)}{dr} \right], \quad (13)$$

while the corresponding MCT result can be obtained from Eq. (12):

$$\eta_{pp}(0)^{\text{MCT}} = \frac{k_B T}{60\pi^2} \int_0^\infty dk k^4 \left[ \frac{S'(k)}{S(k)} \right]^2. \quad (14)$$

By comparing the two expressions given by Eqs. (13) and (14) and by applying Parseval's theorem, one can see that the two results agree when RPA holds. As will be seen from our numerical results presented in the next Section, not only zero-time value of  $\eta_{pp}(t)$ , but also its initial rapid decay is well reproduced by the MCT. Hence, we use Eq. (12) to model the potential part of the time-dependent shear viscosity at all times.

Next, the MCT expression for the mixed kinetic-potential term is given by:[34]

$$\eta_{kp}(t)^{\text{MCT}} = -\frac{m}{15\pi^2} \int_0^\infty dk k \frac{S'(k)}{S(k)^2} \left[ \frac{\partial F(k, t)}{\partial t} \right]^2. \quad (15)$$

In this case, the initial-time value  $\eta_{kp}(0) = 0$ , while the first (linear) term in the short-time expansion of  $\eta_{kp}(t)^{\text{MCT}}$  agrees (under the RPA) with the corresponding exact expansion coefficient.[35] Once again, we employ the MCT expression to describe  $\eta_{kp}(t)$  at all times.

Finally, the MCT result for the kinetic contribution to the time-dependent friction reads:[34]

$$\eta_{kk}(t)^{\text{MCT}} = \frac{m^2}{5\pi^2 k_B T} \int_0^{k_{max}} dk k^2 \left[ \frac{7}{6} C_{tt}^2(k, t) + \frac{1}{3} C_{ll}^2(k, t) + C_{tt}(k, t) C_{ll}(k, t) \right]. \quad (16)$$

The upper cutoff on the wavevector integral,  $k_{max} = (6\pi^2\rho)^{1/3}$ , is determined by the requirement[34] that the initial time value  $\eta_{kk}(0)^{\text{MCT}}$  coincides with the exact value  $\eta_{kk}(0) = \rho k_B T$ . In the above,  $C_{ll}(k, t) = -\ddot{F}(k, t)/k^2$  is the longitudinal current TCF, and  $C_{tt}(k, t)$  is the transverse current TCF. The Laplace transform of the latter (truncated at the second order) is given by:[27, 29]

$$C_{tt}(k, z) = \frac{k_B T/m}{z + \frac{\delta_{1t}(k)}{z + \frac{\delta_{2t}(k)}{z + \tau_t^{-1}(k)}}}, \quad (17)$$

where  $\delta_{it}(k)$  is the initial time value of the  $i^{\text{th}}$  order MF of  $C_{tt}(k, t)$ . The quantities  $\delta_{1t}(k)$  and  $\delta_{2t}(k)$  can be obtained from the first three short-time expansion coefficients of  $C_{tt}(k, t)$ , which are well-known.[31]

In analogy to the continued fraction representation of  $F(k, t)$ , parameter  $\tau_t^{-1}(k)$  is taken to be proportional to  $\sqrt{\delta_{2t}(k)}$ :  $\tau_t^{-1}(k) = \xi\sqrt{\delta_{2t}(k)}$ , with the proportionality factor  $\xi$  determined by requiring that  $C_{tt}(k, t)$  behaves correctly in the hydrodynamic limit:[27, 29, 36]

$$[C_t(k, t)]_{\text{hyd}} = \frac{k_B T}{m} \exp \left[ -\frac{k^2 \eta t}{\rho m} \right], \quad (18)$$

where  $\eta$  is the shear viscosity coefficient. The above requirement yields:

$$\xi = \frac{\eta}{\rho m} \lim_{k \rightarrow 0} \frac{\sqrt{\delta_{2t}(k)}}{\delta_{1t}(k)} k^2 \quad (19)$$

Thus, the calculation of the transverse current TCF requires the knowledge of the shear viscosity coefficient (which is needed to compute parameter  $\xi$  above), while  $\eta$  itself depends on  $C_{tt}(k, t)$  via the kinetic part of the time-dependent shear viscosity. Hence, the calculation of the transverse current TCF and the viscosity coefficient needs to be performed iteratively, in analogy to the calculation of the self-diffusion coefficient and time-dependent friction described earlier.

In order to assess the accuracy of the MCT approach described above, in the next section we compare our theoretical results with the MD data[5–7, 9–11] for self-diffusion and shear viscosity coefficients of GC fluid.

### III. RESULTS

Our results will be presented in terms of dimensionless density and temperature defined by:  $\rho^* = \rho\sigma^3$  and  $T^* = k_B T/\epsilon$ . We also define dimensionless variables for time, self-diffusion coefficient, and shear viscosity coefficient as follows:  $t^* = t(\epsilon/m\sigma^2)^{1/2}$ ,  $D^* = D(m/\epsilon\sigma^2)^{1/2}$ , and  $\eta^* = \eta\sigma^2/\sqrt{m\epsilon}$ .

Before presenting and discussing our results for transport coefficients, we ascertain the accuracy of the HNC closure in calculating structural properties of GC fluid. This is of particular importance because earlier studies have revealed a deep connection between transport coefficients and structural properties, such as excess entropy.[9–11] To this end, we compute from integral equation theory with HNC closure  $g(r)$  for the GC fluid, from which one can readily obtain the two-body contribution to the excess entropy defined as follows:

$$s_2 = -2\pi\rho \int_0^\infty dr r^2 [g(r) \ln g(r) - (g(r) - 1)] \quad (20)$$

MD data[9] and our HNC results for  $-s_2$  are presented in the upper panel of Fig. 1 as a function of fluid density along two isotherms:  $T^* = 0.08$  and  $T^* = 0.2$ . In general, theory is in good agreement with simulations except in the high density range, where it overestimates  $-s_2$  somewhat. Both MD and HNC results show that the negative two-body excess entropy initially increases with density (up to  $\rho^* \sim 0.25$ ), reflecting increasing structural order of the fluid upon its compression. Concomitantly, radial distribution function (not shown) progressively becomes more structured, with the height of its first peak increasing and the second solvation shell gradually developing.[5, 9] In simple fluids, whose interaction potential contains a steeply repulsive core, this familiar type of behavior typically persists throughout the entire liquid density range. By contrast, GC fluid displays qualitatively different behavior at higher densities, whereby its structural order (as measured by  $-s_2$ ) decreases upon further compression, which manifests itself in flattening of solvation shells in  $g(r)$ .[5, 9] This is a consequence of the bounded nature of the GC potential, which allows interparticle overlap. The latter becomes more prominent at higher densities and/or temperatures, ultimately resulting in a high density ideal gas-like structure.[1, 3]

In the high-density regime, GC system behaves as a weakly correlated “mean field fluid”,[13] whose direct correlation function is adequately described by RPA approach. This fact can be illustrated by comparing the results for the initial time value of the time-dependent friction given by Eqs. (7) (exact) and (8) (MCT), which would yield identical results if RPA were exact. The results from the two methods for the dimensionless zero-time value  $\zeta^*(0) = \zeta(0)m\sigma^2/\epsilon$  are shown in the middle panel of Fig. 1 as a function of fluid density along the isotherm  $T^* = 0.08$ . Indeed, the two approaches give quite similar values, and the difference between them diminishes with increasing density. In addition, we have applied the same two methods to compute the  $t^2$  short-time expansion coefficient of the (normalized) time dependent friction,  $\zeta_2(0) = -\frac{d^2\zeta(t)}{dt^2}|_{t=0}/\zeta(0)$ . The corresponding dimensionless result,  $\zeta_2^*(0) = \zeta_2(0)m\sigma^2/\epsilon$ , is presented in the lower panel of Fig. 1. One sees that the two values are remarkably close numerically (except in the low density regime), even though the two expressions (exact and MCT) do not become equivalent under the RPA in this case.

By comparing the density behavior of  $\zeta(0)$  and  $\zeta_2(0)$  shown in Fig. 1, one observes that the latter increases nearly linearly with density throughout the entire range, while for the former fast increase at low densities is followed by slower growth at intermediate  $\rho$  and

**Figure 1**

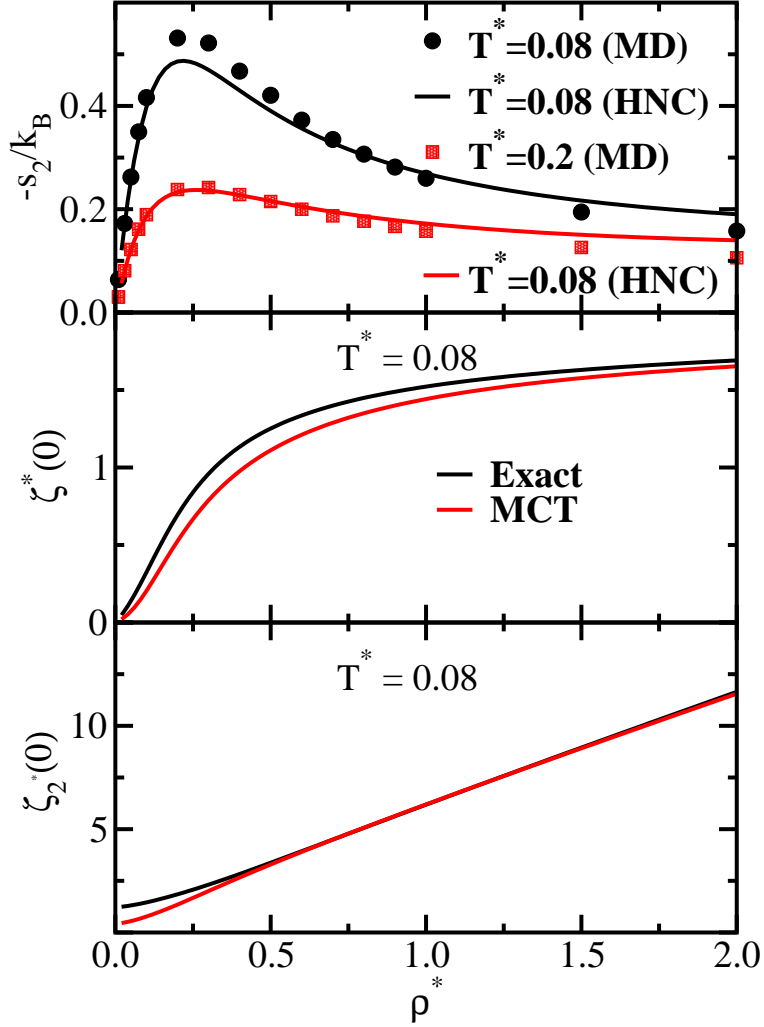


FIG. 1: Upper panel: Simulation and theoretical results for the negative two-body contribution to the excess entropy as a function of fluid density along two isotherms. Middle panel: Initial value of the time-dependent friction as given by exact expression (Eq. (7)) and the MCT approach (Eq. (8)). Lower panel: Short-time expansion coefficient of order  $t^2$  of the normalized time-dependent friction from exact and MCT approaches.

nearly flat behavior in the high-density regime. These results signify that the initial decay rate of the time-dependent friction grows continuously with density, while the growth of its zero-time value with  $\rho$  gradually slows down and nearly saturates.

The above observations can be used to rationalize the density behavior of  $C_v(t)$ , the

**Figure 2**

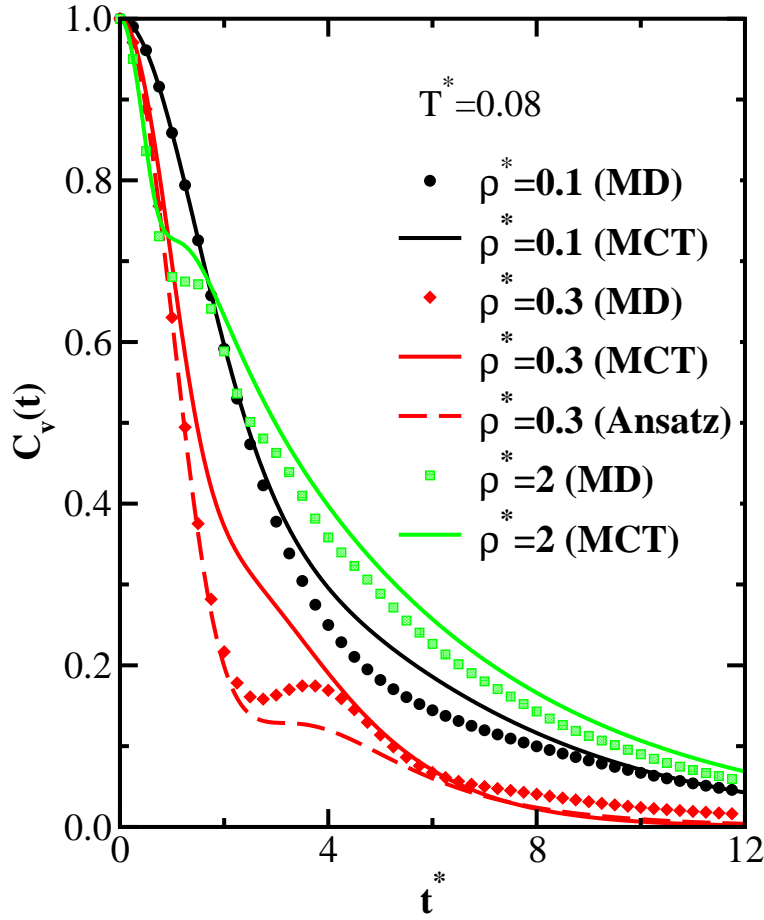


FIG. 2: Simulation and theoretical results for the normalized velocity TCF of a tagged GC particle at  $T^* = 0.08$  at three different densities.

normalized velocity TCF of a tagged GC particle defined by:

$$C_v(t) = \frac{m}{k_B T} \langle v_0^x(t) v_0^x(0) \rangle, \quad (21)$$

where  $v_0^x$  is the  $x$ -component of the tagged particle velocity, and  $\langle \dots \rangle$  denotes the Boltzmann equilibrium average. The Laplace transform of this TCF,  $\tilde{C}_v(z)$ , can be related to the Laplace transform of the time dependent friction as follows:[27, 29]

$$\tilde{C}_v(z) = \frac{1}{z + \tilde{\zeta}(z)}. \quad (22)$$

Simulation[5] and MCT results for  $C_v(t)$  at three different densities along the isotherm  $T^* = 0.08$  are shown in Fig. 2. The most notable feature is biphasic decay of the TCF: except at the lowest density shown, rapid initial decay of  $C_v(t)$  is followed by a “bump” at

intermediate times and a slowly decaying long-time tail, whose amplitude increases markedly with density. The initial decay of the correlation function is governed by its  $t^2$  short-time expansion coefficient, or, equivalently, by the initial time value of its MF, i.e. time dependent friction. As can be seen from the middle panel of Fig. 1, this value initially increases with density, and then gradually saturates. Accordingly, in going from  $\rho^*=0.1$  to  $\rho^*=0.3$  the short-time decay of  $C_v(t)$  becomes considerably faster, while for densities beyond  $\rho^*=0.3$  it stays essentially unchanged. At the same time, as follows from the lower panel of Fig. 1, the short-time decay of  $\zeta(t)$  itself becomes faster with  $\rho$  throughout the entire density range. Faster decaying MF corresponds to slower decaying TCF, which indeed manifests itself in the amplitude of the slowly decaying tail of  $C_v(t)$  growing with density.

In comparing theoretical results with the simulation data presented in Fig. 2, one sees that the MCT approach reproduces biphasic decay of the velocity TCF quite well, with the only significant discrepancy observed at intermediate times for  $\rho^*=0.3$ . In addition to the MCT method, we have also explored an alternative approach to constructing  $C_v(t)$ . [35, 37] This semi-phenomenological approach is based on the short-time expansion of the TCF and is frequently employed in computing transport coefficients via Green-Kubo relation. [35, 37] In particular, one empirical form that is frequently used to model the normalized TCF is written as follows:  $C_v(t) = \cos(bt)/\cosh(at)$ , where parameters  $a$  and  $b$  are chosen in order to reproduce the exact short-time behavior of  $C_v(t)$  up to the term of order  $t^4$ . [35, 37] This ansatz has been successfully applied to calculate diffusion coefficient and other transport properties of simple atomic liquids, whose interaction potential contains a steeply repulsive term at short separations. [35, 37] However, inspection of Fig. 2 reveals that this particular form would not be appropriate in the present case, as it would not be able to capture biphasic decay of the TCF. Instead, we have attempted to model the time-dependent friction via the above phenomenological form:

$$\zeta(t) = \zeta(0) \frac{\cos(bt)}{\cosh(at)} \quad (23)$$

Such approach requires the knowledge of the short-time expansion coefficients of  $\zeta(t)$  up to the order of  $t^4$ , or, equivalently, the expansion coefficients of  $C_v(t)$  up to the order of  $t^6$ . The latter are well-known and will not be reproduced here. [38]

For the density value of  $\rho^*=0.3$ , we display in Fig. 2, alongside with the MCT result,  $C_v(t)$  obtained from the time-dependent friction constructed via Eq. (23). One sees that this phenomenological approach agrees with the MD data even better than the MCT method,

both at short (by construction) and at intermediate times. The performance of ansatz at other densities is equally good and is not shown to avoid overcrowding the graph.

As one last remark concerning velocity TCF, we note that its pronounced biphasic behavior would seemingly suggest applying MCT approach either to  $C_v(t)$  itself,[39] or to its *second-order* MF.[40, 41] We have carried out such calculations, and found, somewhat surprisingly, that the results were less accurate compared to the approach based on the first-order MF outlined above.

We next compute the self-diffusion coefficient of GC fluid via Eq. (2), with time-dependent friction obtained both from MCT (via Eq. (4)) and from ansatz (via Eq. (23)). Our results for  $D^*$  as a function of GC fluid density, together with MD data,[5, 9] are shown in Fig. (3). MCT is generally in good agreement with the simulation, except that it overestimates the value of  $D$  at intermediate densities at  $T^* = 0.08$ , as one could already expect from comparing MCT and MD results for the velocity TCF presented in Fig. (2). By contrast, ansatz systematically under-predicts  $D$  at low and intermediate temperatures. Overall, both methods correctly reproduce the trends in the density dependence of the self-diffusion coefficient observed in the simulations. Specifically, at low and intermediate temperatures,  $D$  initially decreases with  $\rho$ , passes through a minimum (at about the same density, for a given temperature, where  $-s_2$  passes through a maximum), and then keeps increasing throughout the remaining density range. For the highest isotherm shown ( $T^*=1.5$ ), the minimum in  $D$  is barely perceptible, and at still higher temperatures it disappears altogether (likewise for the maximum in  $-s_2$ ). As has been already pointed out,[9] a strong correlation between anomalous density dependencies of  $-s_2$  and  $D$  points to the structural origin of the transport anomalies of GC fluid. This conclusion is further re-inforced by the observation that the density anomaly in  $D$  is successfully captured by the ansatz expression for time dependent friction, which is constructed exclusively from the short-time expansion coefficients of  $\zeta(t)$ . The latter are simply equilibrium averages of certain functions of the interaction potential and its derivatives, i.e. purely structural properties. Some dynamical information does enter the MCT approach, e.g. via the dynamic structure factor, but, again,  $F(k, t)$  was obtained from its continued fraction representation (Eq. (5)), which is completely determined by the short-time expansion coefficients of dynamic structure factor.

Gradual disappearance of the anomalous density behavior of self diffusion coefficient at higher temperatures can also be understood in terms of density dependence of short-time

**Figure 3**

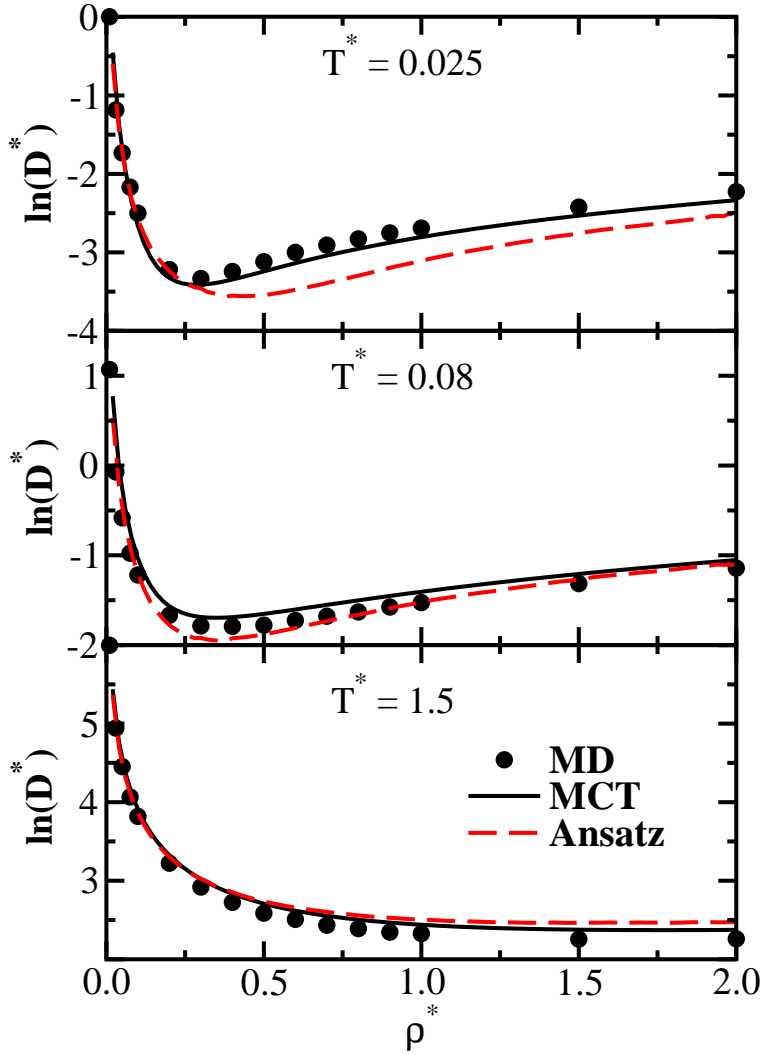


FIG. 3: Simulation and theoretical results for the self-diffusion coefficient of a tagged GC particle as a function of fluid density along three isotherms.

expansion coefficients. In particular, for  $T^* > 1.5$ , the initial value of time dependent friction no longer saturates at high densities, but keeps increasing throughout the entire density range (not shown). As a result, the total time integral of  $\zeta(t)$  keeps increasing, meaning that  $D$  decreases monotonically with  $\rho$ .

Returning to low and intermediate temperatures, the anomalous increase of self-diffusion coefficient with density (and decrease of structural order) is by no means unique to GC fluid; this behavior has been observed for several waterlike model systems,[17–26] as well

Figure 4

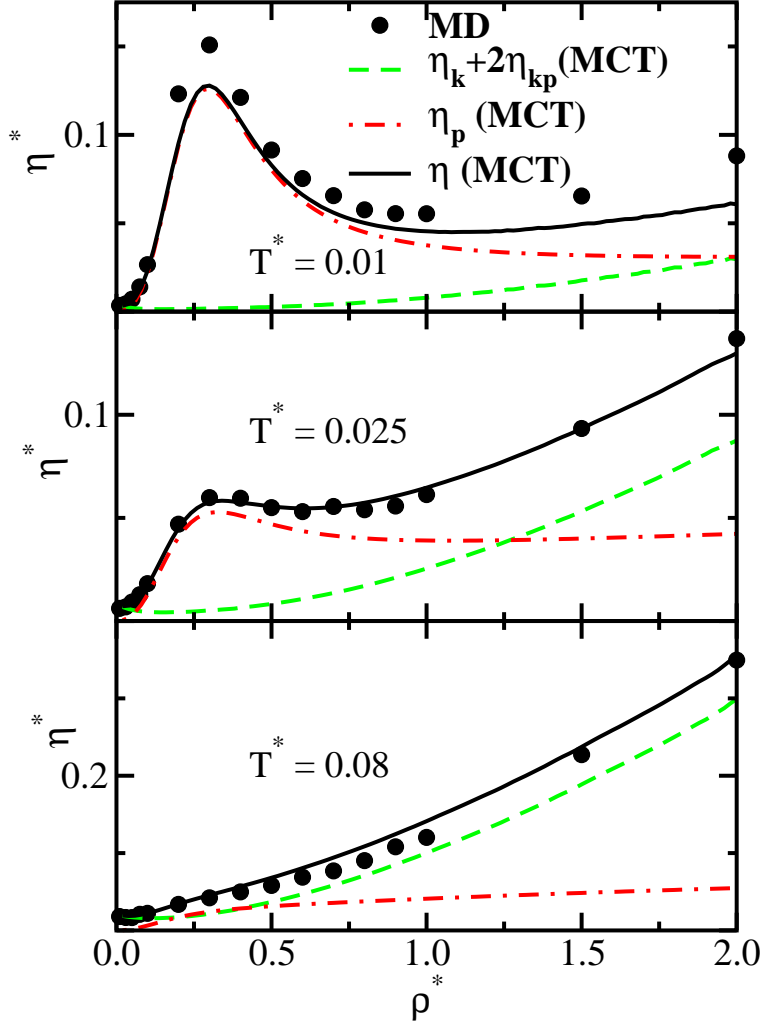


FIG. 4: Simulation and theoretical results for the shear viscosity of GC fluid as a function of fluid density along three isotherms.

as for colloidal systems with short-range attractive interactions.[42] An important difference however, is that for these systems the anomalous structural and dynamical behavior is observed for a limited density range only, after which the system reverts to normal behavior. This is due to the fact that all these model potentials contain a short-range steeply repulsive term, which manifests itself in both structure and dynamics at sufficiently high densities. By contrast, GC potential is bounded, and for this model anomalous behavior persists till the highest density studied.

We next turn to the discussion of shear viscosity coefficient. Simulation[6, 7] and theoretical results for the shear viscosity of GC fluid as a function of fluid density along three isotherms are shown in Fig. 4. Also presented are the MCT results for the components of  $\eta$  arising from the potential term,  $\eta_p$ , and from the sum of kinetic and mixed kinetic-potential terms,  $\eta_k + 2\eta_{kp}$ . At the lowest temperature studied,  $T^* = 0.01$ , the shear viscosity coefficient displays a pronounced anomalous density behavior. Initially,  $\eta$  increases rapidly with  $\rho$ , passes through a maximum around  $\rho^* \sim 0.25$ , exhibits anomalous decrease with density until about  $\rho^* \sim 1$ , and then reverts to normal behavior, i.e. increases with density. This is different from the diffusion anomaly, where  $D$ , after passing through a minimum in the low-density region, keeps increasing with  $\rho$  throughout the entire density range studied. In addition, the temperature range where viscosity anomaly is observed is substantially more narrow compared to the diffusion anomaly. Thus, along the isotherm  $T^* = 0.025$ , the minimum and subsequent maximum in  $\eta$  are barely perceptible, both in MD and MCT results, while at still higher temperatures shear viscosity coefficient increases monotonically with density.

If one considers the decomposition of  $\eta$  into its components, one observes that the anomalous behavior at the lowest temperature is dominated by the potential contribution. Furthermore, after passing through a maximum around  $\rho^* \sim 0.25$ ,  $\eta_p$  keeps decreasing with density for all remaining values of  $\rho$ . By contrast,  $\eta_k + 2\eta_{kp}$  term is monotonically increasing with density. While its magnitude is negligible at low and intermediate densities, it becomes comparable to  $\eta_p$  in the high density region, which produces a minimum in total  $\eta$ . As the temperature is increased, the relative importance of  $\eta_k + 2\eta_{kp}$  term also increases, and eventually its contribution to  $\eta$  becomes dominant, which results in a monotonic increase of the shear viscosity coefficient with density.

Some further light on the origins of the anomalous density behavior of viscosity at low temperatures can be shed by considering the time dependent viscosity given by Eq. (11). The corresponding simulation and theoretical results are shown in Fig. 9 for four different densities along the isotherm  $T^*=0.01$ . One notices that in going from  $\rho^* = 0.1$  to  $\rho^* = 0.3$ , the initial time value  $\eta(0)$  increases dramatically, while the decay rate of  $\eta(t)$  grows only slightly. As a result,  $\eta$ , which is given by the total time integral of  $\eta(t)$ , grows significantly with density in this range. The situation is reversed in the intermediate density range, from  $\rho^*=0.3$  to  $\rho^*=1$ . Here the initial time value grows weakly, while the decay of  $\eta(t)$  becomes

**Figure 5**

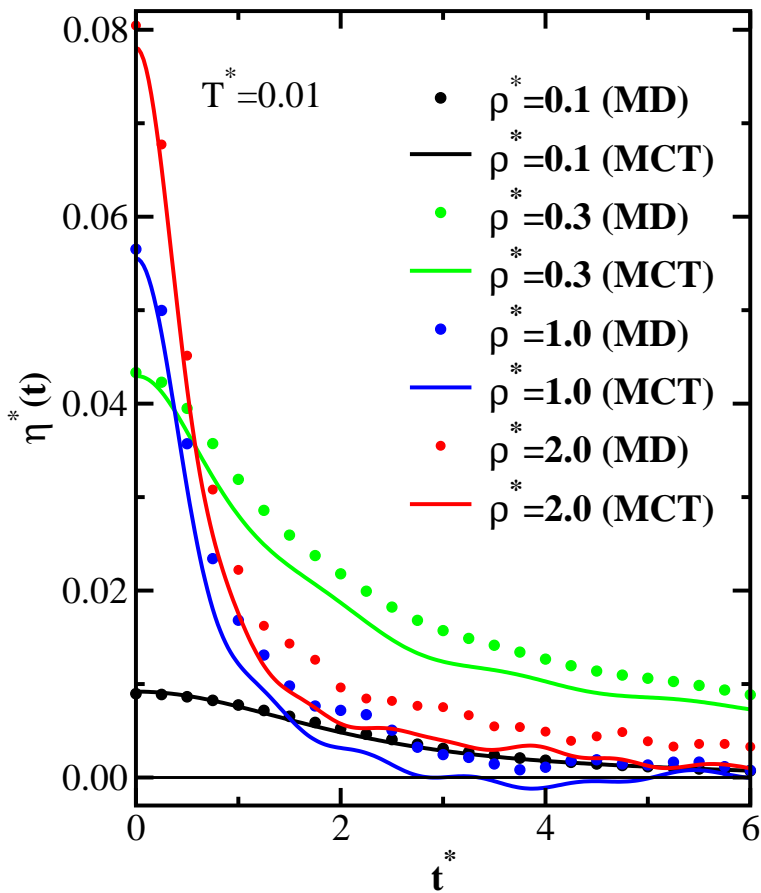


FIG. 5: Simulation and theoretical results for the time-dependent shear viscosity of GC fluid at  $T^*=0.08$  for four different densities.

much faster, thereby producing anomalous density behavior of viscosity in this range. Finally, for densities higher than  $\rho^*=1$ , the initial time value keeps increasing gradually, the initial decay rate does not change significantly, and the amplitude of the long-time tail of  $\eta(t)$  due to mode-coupling effect grows steadily. Hence, the total time integral of  $\eta(t)$  grows with  $\rho$ , and the shear viscosity coefficient reverts to normal density behavior. In terms of comparison between theory and simulation, we note that MCT underestimates the amplitude of the long-time tail somewhat, which results in the under-prediction of  $\eta$  seen in Fig. 4.

In addition to the density behavior of shear viscosity at a given temperature, it is also of interest to analyze its temperature behavior at a given density. To this end, we present in

Figure 6

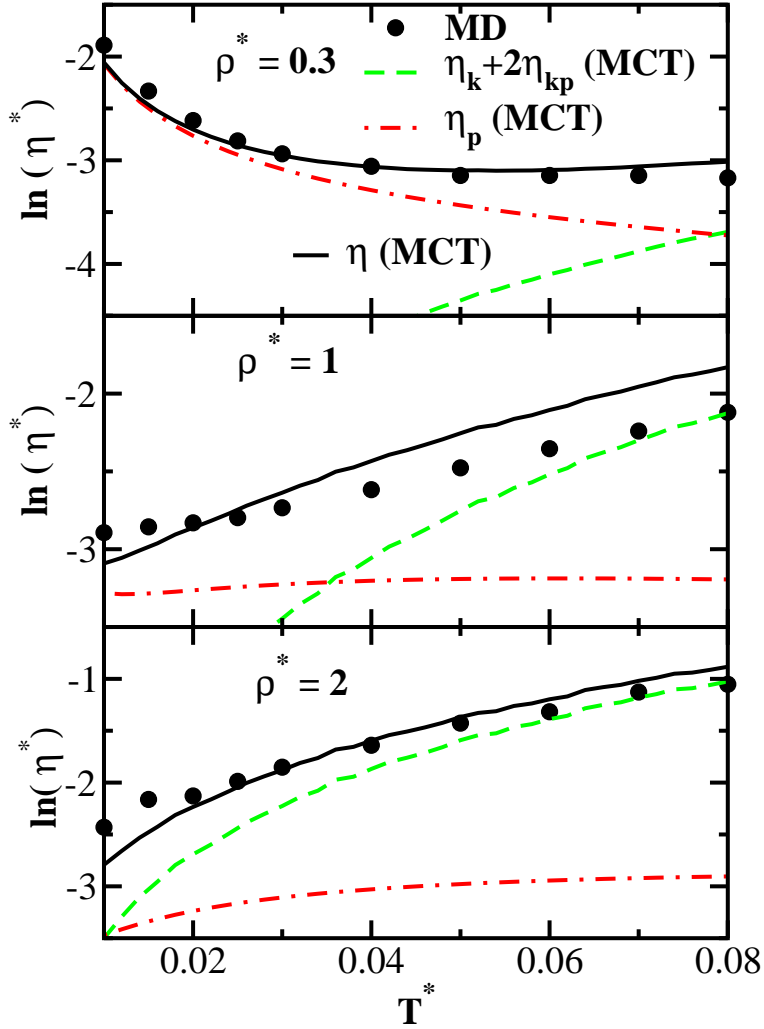


FIG. 6: Simulation and theoretical results for the shear viscosity of GC fluid as a function of fluid temperature along three isochores.

Fig. 6 simulation[6, 7] and theoretical results for the shear viscosity of GC fluid as a function of fluid temperature along three isochores. For the isochore  $\rho^*=0.3$  (where a maximum in  $\eta$  as a function of  $\rho$  is observed), viscosity decreases with temperature at low and intermediate densities. The initial sharp decrease in this  $T$  range is associated with moving away from the liquid-solid phase boundary,[6, 7] and the behavior of  $\eta$  is dominated by the potential term. At higher temperatures,  $\eta_k + 2\eta_{kp}$  term, which is monotonically increasing with  $T$ , becomes comparable in magnitude. As a result, the shear viscosity coefficient passes through

Figure 7

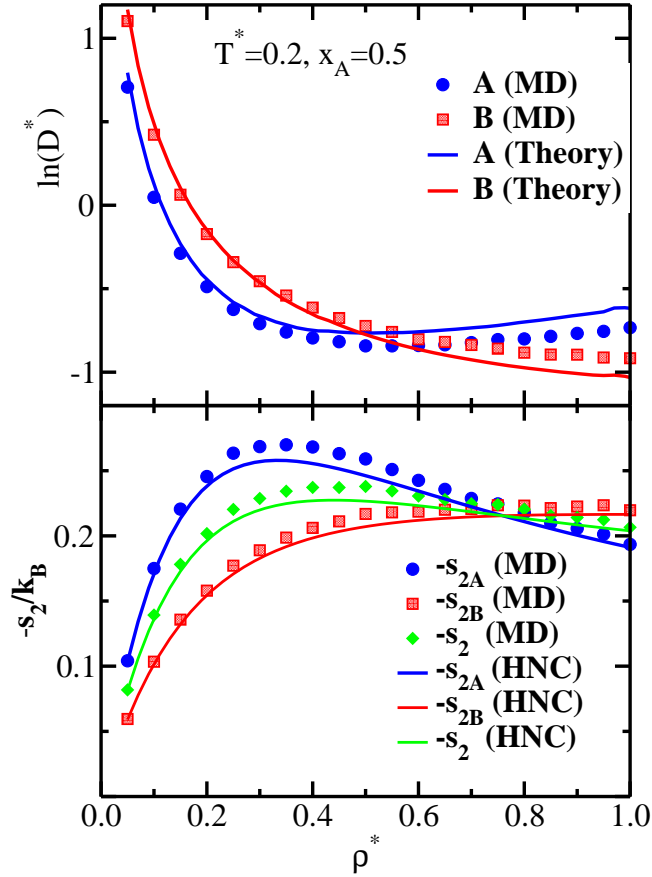


FIG. 7: Upper panel: Simulation and theoretical results for the tracer diffusivities of a binary GC mixture as a function of fluid density along the isotherm  $T^*=0.2$  at the mole fraction  $x_A=0.5$ . Lower panel: negative two-body contributions to the excess entropy of a GC mixture.

a minimum and then grows with temperature.

As the density of GC fluid grows, its freezing temperature drops.[3] As a result, the initial drop of  $\eta$  with  $T$  in the studied temperature range disappears, and  $\eta$  increases monotonically with temperature both for  $\rho^*=1$  and for  $\rho^*=2$ . In the former case, the contributions of kinetic and potential terms to  $\eta$  are comparable, while in the latter case the kinetic term is dominant for all temperatures except for the lowest one.

Finally, in connection to our treatment of time-dependent friction of GC fluid via short-time ansatz, we remark that the short-time expansion coefficients for  $\eta(t)$  have been

reported[35] only up to the term of order  $t^4$ . With this information, one would be able to construct an ansatz of the form given in Eq. (23) only for the time-dependent viscosity itself (or for its individual components defined in Eq. (11)), but not for its first order MF. Given that  $\eta(t)$  at high densities displays a pronounced biphasic behavior similar to that of  $C_v(t)$ , such approach clearly would be inadequate, and we have not pursued it here.

So far, our discussion was limited to a neat GC fluid. However, binary mixtures of GC particles also exhibit structural and dynamical anomalies, both in terms of density and mole fraction behavior. Both thermodynamic[16] and dynamic[11] properties of these mixtures have been studied extensively and the following observations were made. For a binary mixture of particles of two different sizes, at intermediate and high densities, the tracer diffusivity of the larger species increases (and that of the smaller species decreases) either upon increasing the density of the mixture (at fixed mole fraction) or upon increasing the mole fraction of larger species (at a given density). As in the case of a neat GC fluid, a strong correlation was observed between these dynamical anomalies and structural anomalies, as quantified by two-body contributions to excess entropy of individual species.

The aforementioned results for binary mixtures of GC particles were obtained via MD simulations.[11] In the present work, we attempt to calculate the same structural and dynamical properties from a microscopic theory. We consider a two-component GC fluid containing species  $A$  and  $B$ . The pair interaction potential between particles has the form:  $\phi_{ij}(r) = \epsilon_{ij} \exp[-(r/\sigma_{ij})^2]$ , where  $i, j = A, B$ . In order to be able to perform a direct comparison between theory and simulation, we choose a set of parameters used in previous studies:[11, 16]  $\sigma_{BB} = 0.665\sigma_{AA}$ ,  $\sigma_{AB} = (0.5[\sigma_{AA}^2 + \sigma_{BB}^2])^{0.5}$ ,  $\epsilon_{AA} = \epsilon_{BB}$ ,  $\epsilon_{AB} = 0.944\epsilon_{AA}$ . We also assume that the particles of two species have the same mass  $m_A = m_B$ .

As in the case of a neat GC fluid, we compute  $g_{ij}(r)$ , the radial distribution functions of the mixture, from the integral equation theory with HNC closure. The degree of translational structural order of the mixture is quantified via two-body part of the excess entropy given by:[11]

$$s_2 = \sum_i x_i s_{2i}, \quad (24)$$

where  $x_i$  is the mole fraction of species  $i$ , and  $s_{2i}$ , which characterizes the degree of pair structural ordering surrounding particles of species  $i$ , is defined by:[11]

$$\frac{s_{2i}}{k_B} = - \sum_j 2\pi x_j \rho \int_0^\infty dr r^2 [g_{ij}(r) \ln g_{ij}(r) - (g_{ij}(r) - 1)] \quad (25)$$

In order to obtain the tracer diffusivities of the two species from MCT, one needs to construct the corresponding time-dependent friction functions,  $\zeta_i(t)$ , which, in turn, requires the knowledge of the matrix of dynamic and self-dynamic structure factors,  $F_{ij}(k, t)$  and  $F_{sij}(k, t)$ . However, computing  $F_{AB}(k, t)$  from a continued fraction representation is highly problematic,[43] because its zero-time second order time derivative is zero and the sign of the fourth derivative is oscillatory. Instead, one could obtain  $F_{ij}(k, t)$  from a time-dependent density functional theory.[43] However this approach emphasizes long-time hydrodynamic-like behavior of dynamic structure factors, while our results for a neat GC fluid indicate that transport anomalies can be explained on the basis of the short-time behavior of TCFs. In particular the results for  $D$  and  $C_v(t)$  of a neat GC fluid given by a short-time ansatz were for most part comparable in accuracy to the MCT results. Accordingly, instead of constructing MCT for a binary mixture, we have adopted a simpler approach by modeling  $\zeta_i(t)$  via Eq. (23). This approach requires the knowledge of the short-time expansion coefficients of velocity TCFs,  $C_{vi}(t)$ , up to the term of order  $t^6$ . The corresponding expressions have been reported earlier.[44]

We present our results for tracer diffusivities in dimensionless form given by:  $D_i^* = D_i(m_A/\epsilon_{AA}\sigma_{AA}^2)^{1/2}$ , while dimensionless density of the mixture is defined by  $\rho^* = \rho\sigma_{AA}^3$ . Simulation[11] and theoretical results for  $D_i^*$  as a function of fluid density along the isotherm  $T^* = k_B T/\epsilon_{AA}=0.2$  are given in the upper panel of Fig. 7 for the mole fraction  $x_A=0.5$ . While the tracer diffusivity of the larger species displays the same anomalous density behavior as the self-diffusion coefficient of a neat GC fluid (i.e. passes through a minimum around  $\rho^* \sim 0.4$  and then increases with density),  $D_B^*$  decreases monotonically with  $\rho^*$  throughout the entire density range studied. As a result, the curves for the two tracer diffusivities cross at a certain intermediate density, beyond which the mobility of larger particles exceeds that of the smaller particles. Theoretical results agree well with MD data below the crossover density, while above this point ansatz overestimates the tracer diffusivity of the larger species and underestimates that of the smaller species. Still, all the trends in the density behavior of the two diffusivities are reproduced correctly by the theory.

Given that the only input into the theory is the structural information, i.e. the pair distribution functions  $g_{ij}(r)$  entering the expressions for the short-time expansion coefficients, one can expect a strong correlation between structural and dynamical anomalies of a GC binary mixture, similar to that observed for a neat fluid. Indeed, the lower panel of Fig. 7

Figure 8

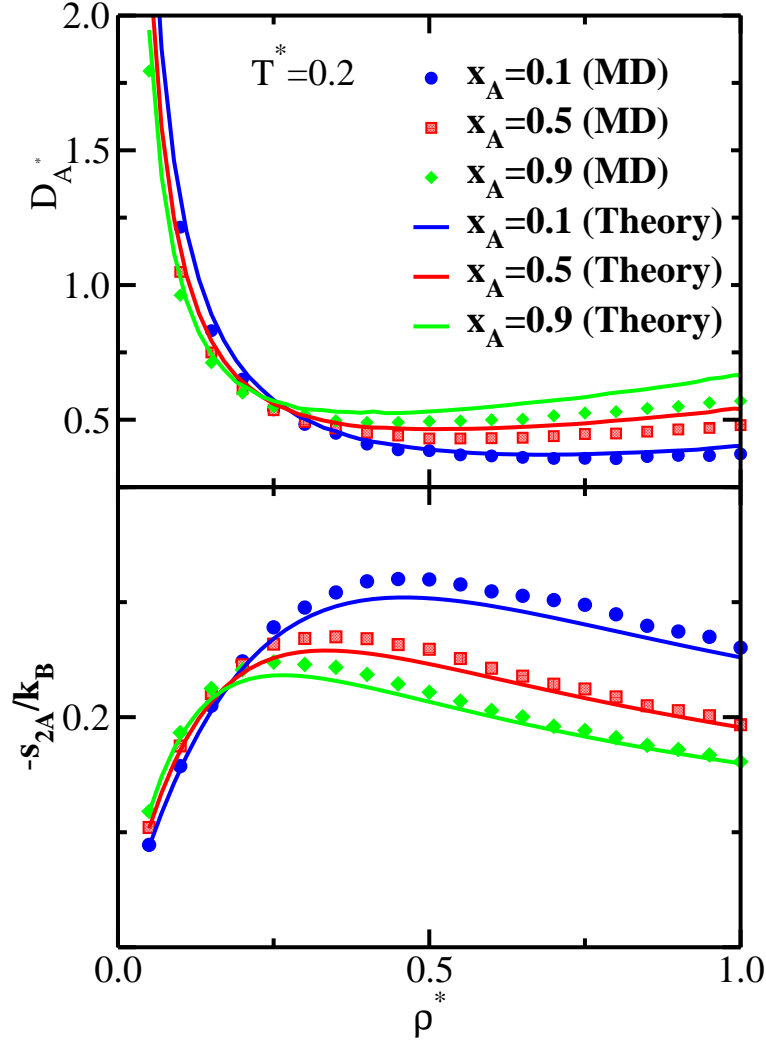


FIG. 8: Upper panel: Simulation and theoretical results for the tracer diffusivity of the larger species of a binary GC mixture as a function of fluid density along the isotherm  $T^*=0.2$  for three values of the mole fraction of A. Lower panel: negative two-body contributions to the excess entropy of the larger species of a binary GC mixture.

displays the two-body contributions to the excess entropy given by Eqs. (24) and (25), and one sees that  $-s_{2A}$  and  $-s_{2B}$  show markedly different density behavior. In analogy to the diffusivity,  $-s_{2A}$  as a function of  $\rho^*$  follows the same pattern as  $-s_2$  of a neat fluid, namely, it initially grows with density, passes through a maximum, and then decreases, reflecting more pronounced overlaps of larger particles at higher densities.[11] By contrast,  $-s_{2B}$  increases

**Figure 9**

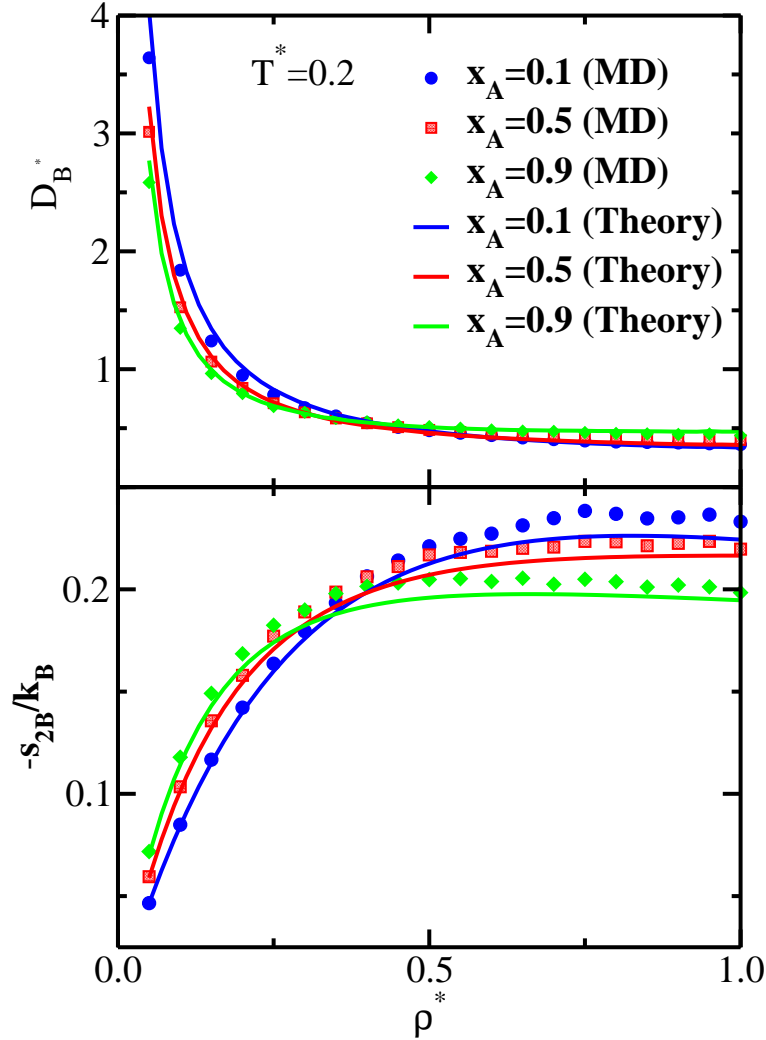


FIG. 9: Upper panel: Simulation and theoretical results for the tracer diffusivity of the smaller species of a binary GC mixture as a function of fluid density along the isotherm  $T^*=0.2$  for three values of the mole fraction of A. Lower panel: negative two-body contributions to the excess entropy of the smaller species of a binary GC mixture.

monotonically with  $\rho$ , which again results in the crossing of the curves for the two species. Theoretical results for  $s_{2i}$  agree well with the MD data,[11] indicating that HNC closure is reliable for calculating the structure of GC mixtures.

Having analyzed the structural and dynamical anomalies of an equimolar GC mixture, we now consider the effect of changing the mole fraction of larger particles on the tracer

diffusivities and structural order metrics of the two species. Tracer diffusivity of the larger species is shown in the upper panel of Fig. 8 as a function of fluid density along the isotherm  $T^*=0.2$  for several values of  $x_A$ ; the corresponding results for  $-s_{2A}$  are shown in the lower panel. Tracer diffusivity and two-body excess entropy of the smaller species at the same conditions are shown in the upper and lower panels of Fig. 9, respectively. One sees that in the low density regime, increase in  $x_A$  results in decreasing tracer diffusivity and increasing structural order metric for both species. As pointed out in the earlier simulation study,[11] this behavior can be expected, because increasing mole fraction of the larger species results in higher packing fraction of the fluid. By contrast, at higher densities, larger values of  $x_A$  correspond to more overlaps between particles, which translates into lower values of  $-s_{2i}$  and higher values of  $D_i$  for both species. While the trends in the mole fraction behavior of  $-s_{2i}$  and  $D_i$  are the same for both species, the switch from expected to anomalous dependence on  $x_A$  occurs earlier (i.e. at a lower value of bulk density) for the larger species. Once again, theory successfully captures all the trends observed in simulations, even though there are minor quantitative discrepancies, mostly at high densities.

As a final remark on GC mixtures, we note that for a given density and temperature one might expect anomalous (i.e. nonlinear) dependence of shear viscosity on the mole fraction  $x_A$ . [43] Given that our short-time ansatz is inadequate for modeling time-dependent viscosity, we cannot verify this conjecture presently. One possible approach to this problem would be to obtain dynamic structure factors  $F_{ij}(k, t)$  for the mixture from a fully self-consistent MCT framework. [45] This will be the subject of future investigation.

#### IV. CONCLUSION

In summary, we have reported a theoretical study of structural and dynamical anomalies of a neat GC fluid and GC binary mixture. As has been discussed previously in the literature,[9–11] essentially all the observed anomalies can be traced back to the fact that GC potential is bounded and, as such, allows interparticle overlap, which becomes more and more prominent at higher densities. We have employed integral equation theory to compute the GC liquid structure and both MCT approach and short-time ansatz for MFs to obtain its transport coefficients. Theory was successful in reproducing anomalous density behavior of both diffusion coefficient and shear viscosity, where the former increases and the

latter decreases with density. One major difference between the two is that viscosity displays anomalous behavior over a limited density range only, following which it again increases with density, while diffusion anomaly persists over the entire density range studied. This fact was rationalized by noting that viscosity can be split into potential and kinetic contributions, with the former displaying anomalous density dependence and the latter behaving normally. With increasing density and/or temperature, the relative importance of the kinetic term increases, and viscosity reverts from anomalous to normal density behavior.

A deep connection between structural and dynamical anomalies uncovered in earlier studies[9–11] has been reconfirmed by noting that both density and mole fraction anomalous behavior of diffusion could be described via a short-time ansatz for a time-dependent friction, with the latter constructed from structural data only. One remaining open question concerns the mole fraction dependence of shear viscosity of a GC mixture, it will be the subject of future research.

## V. ACKNOWLEDGMENT

The authors would like to thank Profs. T. M. Truskett and H.-O. May and Drs. W. P. Krekelberg and M. J. Pond for sending the simulation data. One of us (S. A. E.), acknowledges support from the Alexander von Humboldt foundation, Germany.

- 
- [1] F. H. Stillinger, *J. Chem. Phys.* **65**, 3968 (1976).
  - [2] F. H. Stillinger and D. K. Stillinger, *Physica A* **244**, 358 (1997).
  - [3] A. Lang, C. N. Likos, M. Watzlawek, and H. Lowen, *J. Phys. Cond. Matt.* **12**, 5087 (2000).
  - [4] S. Prestipino, F. Saija, and P. V. Giaquinta, *J. Chem. Phys.* **123**, 144110 (2005).
  - [5] P. Mausbach and H.-O. May, *Fluid Phase Equilibria* **249**, 17 (2006).
  - [6] P. Mausbach and H.-O. May, *Z. Phys. Chem.* **223**, 1035 (2009).
  - [7] H.-O. May and P. Mausbach, *Phys. Rev. E* **76**, 031201 (2007).
  - [8] A. Ahmed, P. Mausbach, and R. J. Sadus, *J. Chem. Phys.* **131**, 224511 (2009).
  - [9] W. P. Krekelberg, T. Kumar, J. Mittal, J. R. Errington, and T. M. Truskett, *Phys. Rev. E* **79**, 031203 (2009).

- [10] W. P. Krekelberg, M. J. Pond, G. Goel, V. K. Shen, J. R. Errington, and T. M. Truskett, *Phys. Rev. E* **80**, 061205 (2009).
- [11] M. J. Pond, W. P. Krekelberg, V. K. Shen, J. R. Errington, and T. M. Truskett, *J. Chem. Phys.* **131**, 161101 (2009).
- [12] B. M. Mladek, G. Kahl, and M. Neumann, *J. Chem. Phys.* **124**, 064503 (2006).
- [13] A. A. Louis, P. G. Bolhuis, and J. P. Hansen, *Phys. Rev. E* **62**, 7961 (2000).
- [14] H. H. Wensink, H. Löwen, M. Rex, C. N. Likos, and S. van Teefelen, *Comp. Phys. Comm.* **179**, 77 (2008).
- [15] F. Eurich, A. Karatchentsev, J. Baschnagel, W. Dieterich, and P. Maass, *J. Chem. Phys.* **127**, 134905 (2007).
- [16] A. J. Archer and R. Evans, *Phys. Rev. E* **64**, 041501 (2001).
- [17] P. C. Hemmer and G. Stell, *Phys. Rev. Lett.* **24**, 1284 (1970).
- [18] M. R. Sadr-Lahijany, A. Scala, S. V. Buldyrev, and H. E. Stanley, *Phys. Rev. Lett.* **81**, 4895 (1998).
- [19] E. A. Jagla, *J. Chem. Phys.* **111**, 8980 (1999).
- [20] G. Franzese, G. Malescio, A. Skibinsky, S. V. Buldyrev, and H. E. Stanley, *Nature* **409**, 692 (2001).
- [21] Z. Yan, S. V. Buldyrev, N. Giovambattista, and H. E. Stanley, *Phys. Rev. Lett.* **95**, 130604 (2005).
- [22] P. Kumar, S. V. Buldyrev, F. Sciortino, E. Zaccarelli, and H. E. Stanley, *Phys. Rev. E* **72**, 021501 (2005).
- [23] J. Mittal, J. R. Errington, and T. M. Truskett, *J. Chem. Phys.* **125**, 076102 (2006).
- [24] A. B. de Oliveira, P. A. Netz, T. Colla, and M. C. Barbosa, *J. Chem. Phys.* **124**, 084505 (2006).
- [25] J. R. Errington, T. M. Truskett, and J. Mittal, *J. Chem. Phys.* **125**, 244502 (2006).
- [26] S. A. Egorov, *J. Chem. Phys.* **128**, 174503 (2008).
- [27] U. Balucani and M. Zoppi, *Dynamics of the Liquid State* (Clarendon, Oxford, 1994).
- [28] S. Bhattacharyya and B. Bagchi, *J. Chem. Phys.* **106**, 1757 (1997).
- [29] J. P. Hansen and I. R. McDonald, *Theory of Simple Liquids, 2nd ed.* (Academic, London, 1986).
- [30] S. W. Lovesey, *J. Phys. C* **4**, 3057 (1971).

- [31] R. Bansal and K. N. Pathak, *Phys. Rev. A* **15**, 2519 (1977).
- [32] S. Bhattacharyya and B. Bagchi, *J. Chem. Phys.* **109**, 7885 (1998).
- [33] M. P. Allen and D. J. Tildesley, *Computer Simulation of Liquids* (Clarendon, Oxford, 1987).
- [34] T. Franosch and W. Götze, *Phys. Rev. E* **57**, 5833 (1998).
- [35] R. K. Sharma, K. Tankeshwar, and K. N. Pathak, *J. Phys.: Condens. Matter* **7**, 537 (1995).
- [36] R. Bansal, *Phys. Rev. A* **16**, 2191 (1977).
- [37] S. A. Egorov, M. D. Stephens, A. Yethiraj, and J. L. Skinner, *Mol. Phys.* **88**, 477 (1996).
- [38] K. Tankeshwar, K. N. Pathak, and S. Ranganathan, *J. Phys. C* **20**, 5749 (1987).
- [39] T. Gaskell and S. Miller, *J. Phys. C* **11**, 3749 (1978).
- [40] J. Bosse, W. Götze, and A. Zippelius, *Phys. Rev. A* **18**, 1214 (1978).
- [41] S. A. Egorov, *J. Chem. Phys.* **119**, 4798 (2003).
- [42] J. Mittal, J. R. Errington, and T. M. Truskett, *J. Phys. Chem. B* **110**, 18147 (2006).
- [43] G. Srinivas, A. Mukherjee, and B. Bagchi, *J. Chem. Phys.* **114**, 6220 (2001).
- [44] R. K. Sharma and K. Tankeshwar, *J. Chem. Phys.* **108**, 2601 (1998).
- [45] E. Flenner and G. Szamel, *Phys. Rev. E* **72**, 031508 (2005).